An Alternative Method for the Identification of the Modal Damping Factor based on the Dissipated Energy

D. Montalvão[a,b,1], J.M.M. Silva[b]

[a] School of Engineering and Technology, University of Hertfordshire, College Lane Campus, Hatfield, AL10 9AB, United Kingdom

[b] Department of Mechanical Engineering, Instituto Superior Técnico, Technical University of Lisbon, Av. Rovisco Pais, 1049-001 Lisbon, Portugal

Abstract

The identification of the modal parameters from frequency response functions is a subject that is not new. However, the starting point often comes from the equations that govern the dynamic motion. In this paper, a novel approach is shown, resulting from an analysis that starts on the dissipated energy per cycle of vibration. Numerical and experimental examples were used in order to assess the effectiveness of the proposed method. It was shown that, for lightly damped systems with conveniently spaced modes, it produced quite accurate results when compared to those obtained from the method of the inverse. The technique also proved to be simple enough to be used for quick estimates of the modal damping factors. Finally, this paper is a contribution to modal analysis and identification methods, as the developed technique has never been proposed before.

Keywords: experimental modal analysis (EMA); modal identification; method of the inverse; dissipated energy.

1. Introduction

Modal identification seeks to obtain the global and local characteristics of vibrating structures using experimental data. This technique may be used either to obtain the global characteristics (natural frequencies and damping), to directly derive a mathematical model of the structure or to improve an existing finite element model through what is frequently called *updating*. The

---

[1] Corresponding author. Tel.: +44 (0)1707 285387.

E-mail address: d.montalvao@herts.ac.uk.

interest of modal identification procedures is acknowledged by the scientific community and many authors have addressed this problem, mainly since the early seventies of the past century [1]. The proposed modal identification procedures cover different levels of sophistication and, in almost all cases, need the use of special software that may not be easy to obtain.

In the past few years, attention has been more focused on Operational Modal Analysis (OMA) rather than in the more traditional Experimental Modal Analysis (EMA). Examples of later developments in OMA identification methods can be found, for instance, in [2-5]. In terms of EMA, later publications are more concerned with Engineering applications, as can be seen, for instance, in [6-7]. OMA deals with operational deflection shapes and many often make use of output-only measurements, this meaning that excitation loads are unknown. EMA makes use of both input forces and output responses in order to determine modal parameters and mode shapes. Numerous modal identification algorithms have been developed in the past thirty years [8]. However, even if in the past recent years not many advances have been seen in terms of EMA modal identification methods, there are a few interesting results that can still be derived.

If the sole objective is the determination of the global modal characteristics, it is possible to use simple approaches producing quick estimates of the desired information. This issue is addressed in this paper where a new simple method is proposed, based on the dissipated energy per cycle of vibration. The proposed methodology is a robust estimator, provided the systems under analysis are not heavily damped and the modes are sufficiently separated so that their mutual interference may be assumed as negligible.

This paper presents the proposed new methodology and applies it to both numerical and experimental examples, showing that it yields reasonably accurate results.

2. Theoretical development

2.1. Definitions

The concept of a complex stiffness in vibration problems with viscous or structural (hysteretic) damping is something that has been known for decades. Most often the complex stiffness is defined as the sum of the stiffness itself (k, real part) and the damping coefficient (d, imaginary part):

$$k^* = k + id \tag{1}$$

To find the real and imaginary parts of the complex stiffness, it is easier if the more conventional viscous damping model is firstly introduced. The well-known second order differential equation of motion - for a single degree-of-freedom system (SDOF) - is given by:

$$m\ddot{x} + c\dot{x} + kx = Fe^{i\omega t} \tag{2}$$

where m is the mass, c is the viscous damping coefficient, k is the stiffness, F is the amplitude of the oscillatory force and t is the time variable. When excited by an harmonic force with frequency ω, it can easily be proven (and most fundamental texts on vibration theory show it, for instance [1,9]) that for each vibration cycle the system dissipates – through its viscous damper – a quantity of energy directly proportional to the damping coefficient, the excitation frequency and the square of the response amplitude X:

$$W_{diss} = \int_0^T f\dot{x}dt = \pi c\omega X^2 \tag{3}$$

where $T = 2\pi/\omega$ is the time period of oscillation. However, experimental evidence from tests performed on a large variety of materials show that the damping due to internal friction (material hysteresis) is nearly independent of the forcing frequency but still proportional to the square of the response amplitude [10], i. e.:

$$W_{diss} \propto CX^2 \tag{4}$$

where C is a constant. Therefore, from Eqs. (3) and (4) the equivalent damping coefficient is:

$$c = \frac{C}{\pi\omega} = \frac{d}{\omega} \tag{5}$$

with $d = C/\omega$. In such conditions, Eq. (2) can be re-written as:

$$m\ddot{x} + \frac{d}{\omega}\dot{x} + kx = Fe^{i\omega t} \tag{6}$$

As $\dot{x} = i\omega x$ for a harmonic vibration, the previous equation may be re-written as:

3

$$m\ddot{x} + k(1 + i\eta)x = Fe^{i\omega t} \tag{7}$$

where

$$\eta = d/k \tag{8}$$

is known as the hysteretic damping ratio or damping loss factor. The quantity:

$$k^* = k(1 + i\eta) \tag{9}$$

is the same complex stiffness as initially described in Eq. (1).

The latter formulation (7) leads to the conclusion that the dissipated energy per cycle of vibration is independent of the forcing frequency.

2.2. A novel approach to the determination of the hysteretic damping coefficient in SDOF systems

The experimental measurement of the hysteretic damping factor can be carried out by means of cyclic force-displacement tests in the elastic domain [11]. Following the reasoning presented earlier, it is easy to show that the energy dissipated per cycle of oscillation is given by the ellipse area of the force *vs* displacement plot during a complete cycle. Rearrangement of Eqs. (3), (5) and (8) lead to:

$$W_{diss} = \pi dX^2 = \pi\eta kX^2 \tag{10}$$

This area, the integral of the force along the displacement, corresponds to the non-conservative work done per cycle. In other words, in a plot of force *vs* displacement at a given frequency, damping can be seen as a mechanism that introduces a lag between force and displacement and shows up as an elongated ellipsis [10,11]. In fact, from [12], it can also be shown that the dissipated energy can be written as:

$$W_{diss} = \pi FX \sin\theta \tag{11}$$

where θ is the phase angle between the force and the displacement response. From Eqs. (10) and (11) a relationship between the hysteretic damping coefficient, the displacement, the force and the phase angle can be established as:

$$d = \frac{F}{X} sin(\theta)$$

(12)

For harmonic motion, the ratio between the force and the displacement is a transfer function often referred to as Dynamic Stiffness [1]. Usually, in experimentation, one measures the Receptance instead, which is the inverse of the Dynamic Stiffness:

$$\alpha(\omega) = \frac{x(\omega)}{f(\omega)}$$

(13)

The quantities $x(\omega)$ and $f(\omega)$ are the complex response and force with amplitudes $X(\omega)$ and $F(\omega)$, respectively, both a function of the angular frequency ω. If the amplitude of the receptance is represented by $H(\omega)$, then Eq. (12) can be re-written more conveniently as:

$$sin(\theta) = d \cdot H(\omega)$$

(14)

This equation suggests that the hysteretic damping coefficient d can be simply determined from the measurement of the amplitude and phase of the receptance. Once the stiffness is known, Eq. (8) allows determining the hysteretic damping factor η.

2.3. Determination of the damping factor from the damping coefficient in SDOF systems

Considering a SDOF system, the receptance (13) may be written as [1]:

$$\alpha(\omega) = \frac{1}{(k - \omega^2 m) + id}$$

(15)

If the method of the inverse is applied, one obtains:

$$\frac{1}{\alpha(\omega)} = (k - \omega^2 m) + id$$

(16)

Where the imaginary part is:

5

$$Im\left(\frac{1}{\alpha(\omega)}\right) = d \tag{17}$$

Eq. (17) is an alternative form to Eq. (14) presented in this paper and will be used for comparison purposes. This equation has been represented before in [9] on the Argand plane. A least-squares best fit of a straight line was suggested to be constructed through the data points in order to estimate the damping parameter from the interception of the line with the imaginary axis.

Consider, now, the real part of Eq. (16):

$$Re\left(\frac{1}{\alpha(\omega)}\right) = k - \omega^2 m \tag{18}$$

This Eq. (18) is a straight line of the real part of the dynamic stiffness with respect to ω^2, with a negative slope m and the interception of the line with the y-axis leads to k. Once these values are known, the damping factor can finally be determined from (8) – whether the damping coefficient has been determined by (14) or (17) - and the natural frequency can be estimated from:

$$\omega_n = \sqrt{\frac{k}{m}} \tag{19}$$

2.4. Generalisation to MDOF systems

The previous approach is not very useful since most real systems are multiple degree-of-freedom (MDOF), so it must be generalised. It is well known that, in a MDOF, the overall receptance is the sum of each individual degree-of-freedom contribution:

$$\alpha(\omega) = \sum_r \frac{m_r \bar{A}_r}{k_r - m_r \omega^2 + id_r} \tag{20}$$

where $\bar{A}_r$ is the complex modal constant for mode r and each mode has its own modal stiffness k_r, modal mass m_r and modal damping coefficient d_r.

A few simplifications are now convenient. Consider that the numerator on Eq. (20) can be treated as a real quantity. At the vicinity of a resonance ω_r, Eq. (20) is mostly dominated by the corresponding mode r. In this case, Eq. (20) is approximated by:

$$\alpha(\omega \to \omega_r) \cong \frac{m_r A_r}{k_r - m_r \omega^2 + i d_r} + \bar{C}_r \tag{21}$$

in which $\bar{C}_r$ is a complex constant that takes into consideration the influence of all other modes at the vicinity of mode r. Also, consider that the modes are sufficiently spaced and that the receptance is available at points that are far away from nodal lines. In such a case, the influence from other modes is small when compared to the resonant mode and the following approximation can be made:

$$\alpha(\omega \to \omega_r) \cong \frac{m_r A_r}{k_r - m_r \omega^2 + i d_r} \tag{22}$$

Eq. (22) resembles the equation of a SDOF with a real modal constant.

If the method of the inverse is applied, the simplification that the modal constant is a real number leads to:

$$\frac{1}{\alpha(\omega \to \omega_r)} \cong \frac{(k_r - \omega^2 m_r)}{m_r A_r} + i \frac{d_r}{m_r A_r} \tag{23}$$

where the real part is given by:

$$Re\left(\frac{1}{\alpha(\omega \to \omega_r)}\right) \cong \frac{k_r}{m_r A_r} - \omega^2 \frac{m_r}{m_r A_r} \tag{24}$$

The natural frequency can now be determined in a similar away to (19) and is independent of the modal constant:

$$\omega_r = \sqrt{\frac{k_r/(m_r A_r)}{m_r/(m_r A_r)}} = \sqrt{\frac{k_r}{m_r}} \tag{25}$$

Thus, as long as the modes are sufficiently spaced in frequency and the modal constant is real (or its imaginary part is small in comparison to its real counterpart), this method suggests that the natural frequencies can be determined with a reasonable degree of accuracy.

For the determination of the damping coefficient, the reasoning is similar. Again, it is assumed that an MDOF can be described as the sum of the contribution from several independent

SDOFs. In such a case, and taking into consideration (11), the overall dissipated energy at each frequency ω is:

$$W_{diss}(\omega) = \sum_r W_{diss,r}(\omega) = \sum_r \pi F(\omega) X_r(\omega) \sin(\theta_r(\omega)) \qquad (26)$$

For lightly damped SDOF systems, the phase $\theta(\omega)$ of the receptance has a value close to zero before the resonance and 180° after the resonance. In any of these two cases, $sin(\theta(\omega)) \cong 0$. However, at the resonant frequency the phase $\theta(\omega_r)$ switches from 0° to 180° assuming values close to 90°, which means that, at the resonant frequency, $sin(\theta(\omega_r)) \cong 1$. In other words, near a natural frequency, the dissipated energy (26) assumes a form that resembles the one of a SODF:

$$W_{diss}(\omega \rightarrow \omega_r) = \pi F(\omega) X_r(\omega) \sin(\theta_r(\omega)) + E \qquad (27)$$

in which E is a constant that takes into consideration the energy that is being dissipated by other modes. For lightly damped systems $sin(\theta(\omega)) \cong 0$ and E can be assumed close to zero. This behaviour of $sin(\theta(\omega))$ also suggests that Eq. (14) can be used to determine the damping coefficient with a certain degree of accuracy in the vicinity of a mode, at least for lightly damped systems and as long as the mode shapes are sufficiently spaced.

3. Numerical Examples

3.1. Numerical Setup

The performance of Eq. (14) was compared to Eq. (17). For a matter of simplicity, these methods are referred as method of the "slope" and method of the "intersection" throughout this paper, respectively. In both cases, the modal hysteretic damping factors were determined using (8). Each modal stiffness and modal mass were estimated from a least-squares best fit from Eq. (24), in which the stiffness parameter is estimated from the interception of the line with the imaginary axis and the modal parameter is estimated from the slope of the line. The natural frequency was finally determined from (25).

A set of different numerical examples were built using Eq. (20), but covering many different scenarios[2]. The different scenarios are described in table 1.

Table 1 Numerical examples analysed during sections 3.2 to 3.6.

Case / Section	Mode 1				Mode 2				Random Noise
	Modal Constant 1		$f(Hz)$	η	Modal Constant 2		$f(Hz)$	η	
	Real	Imag			Real	Imag			
3.2	10e3	-	20	0.05	-	-	50	0.01	-
3.3	10e3	-	20	0.05	-5e3	-	50	0.01	-
3.4	10e3	10e3	20	0.05	-	-	50	0.01	-
3.5	10e3	10e3	20	0.5	-5e3	-5e3	50	0.01	-
3.6	10e3	10e3	20	0.5	-5e3	-5e3	50	0.01	±10%

In the following sections, 3.2 to 3.6, the results for the identification of the natural frequencies and hysteretic damping factors are discussed. In particular, four types of pictures are analysed:

- Plot of the amplitude of the receptance *vs* frequency;
- Plot of $sin(\theta)$ *vs* the amplitude of the receptance (Eq. (14));
- Plot of the real part of the dynamic stiffness *vs* the square of the angular frequency (Eq. (24));
- Plot of the imaginary part *vs* the real part of the the dynamic stiffness.

In terms of the parameters that are analysed, the hysteretic damping factor and the natural frequency were selected, instead of other parameters, such as the modal stiffness or modal mass, since the former are easier to interpret in modal analysis.

3.2. SDOF with a Real Modal Constant

---

[2] The modal constants, natural frequencies and hysteretic damping factors may not have any real physical meaning and were chosen just to fit the specific purpose of the demonstrations.
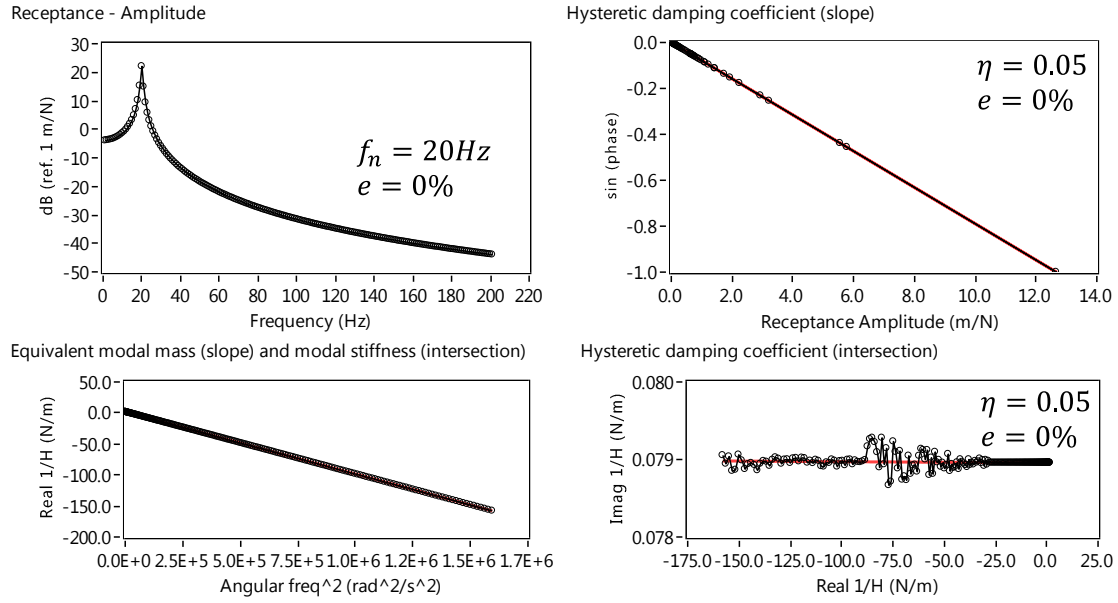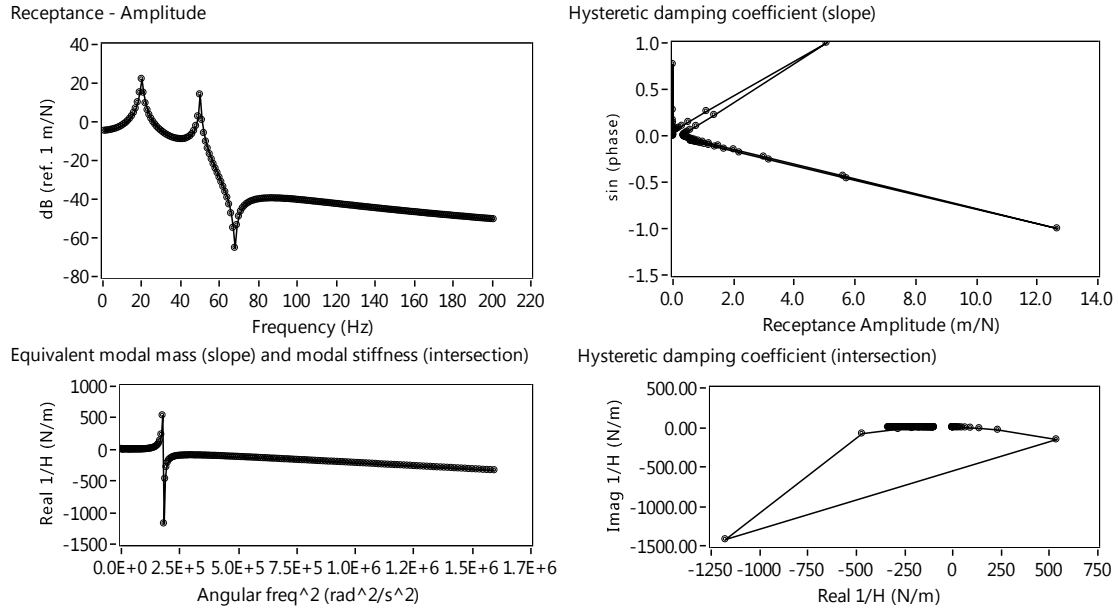
Fig. 1. Numerical results of an SDOF with a real modal constant - $f = 20Hz$ and $\eta = 0.05$.

The results for the numerical example of an SDOF with a real modal constant are presented in Fig. 1. First of all, it can be observed that the plot of $sin(\theta(\omega))$ *vs* the amplitude of the receptance (top right plot) is a straight line intersecting the y-axis at the origin. This suggests that the hysteretic damping coefficient d in Eq. (14) actually is the slope of this line, which can be estimated constructing a least-squares best fit through the data points. The hysteretic damping factor is then determined from (8), after a least-squares best fit is constructed through the data points on the bottom left corner plot (real part of the dynamic stiffness vs the angular frequency to the power of 2).

For this numerical example, both the "slope" and "intersection" methods produced exact solutions, although the method of the "intersection" is slightly sensitive to numerical instability.
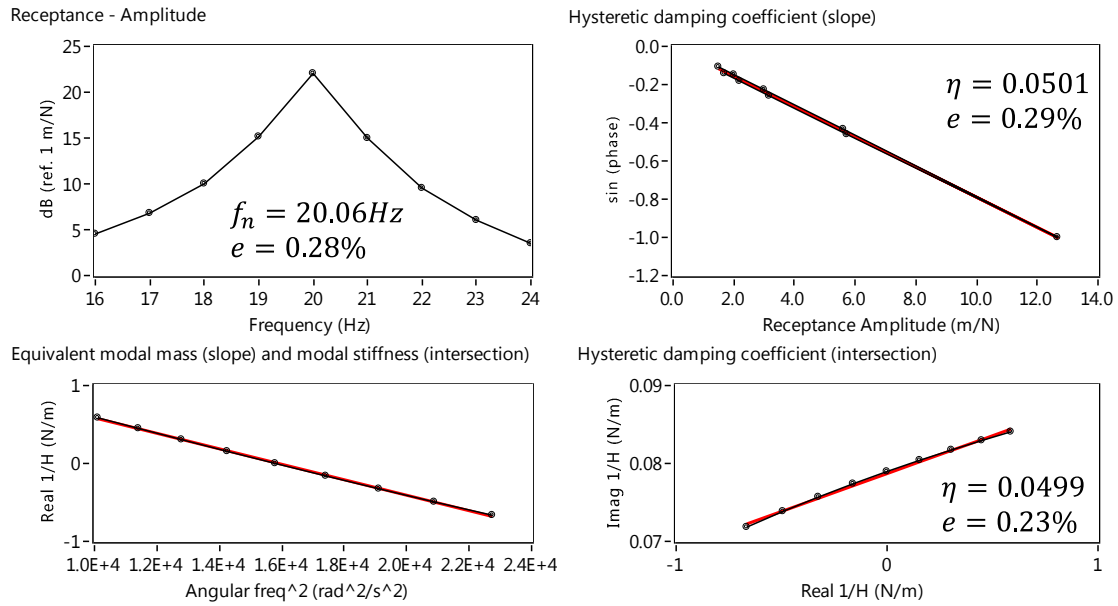
3.3. MDOF with Real Modal Constants

Fig. 2. Numerical results of an MDOF with real modal constants - $f_1 = 20Hz$, $f_2 = 50Hz$, $\eta_1 = 0.05$ and $\eta_2 = 0.01$.

For a 2 DOF system with real modal constants, the results presented in Fig. 2 show that it is not possible to make the identification of the modal parameters using the whole frequency span at the same time. This problem is not new and has been circumvented in many other methods by "zooming in" a region in the plot around the natural frequencies'. However, one interesting feature of the method of the "slope" is that the two modes are visible on the upper right corner plot. This is due to the modal constants having different signals and, as a consequence, the slopes have different signals as well.

Figs. 3 and 4 are close-ups at 20Hz and 50Hz, the two resonances, respectively. In these two cases the hysteretic damping factor and natural frequency are determined, again, with a high degree of accuracy (<1% error), regardless of the method used.

It is important to notice, nonetheless, that a different number of points was selected for the modal identification from Fig. 3 to Fig. 4. One of the reasons is that the bottom-left corner plot in Fig. 4 is not "as linear" as the corresponding one in Fig. 3. Also, the top-right corner plot in Fig. 4 is not "as sharp" as the corresponding one in Fig. 3. This is because in MDOF systems modes affect one another. Because of this lack of sharpness in the "slope" method, the identification was carried out centred at the natural frequency (same number of data points to the left and to the right). This suggests that the method of the "slope" is more sensitive to the

experience of the user than the method of the "intersection", as the latter one does not need to be centred at the natural frequency.

Fig. 3. Numerical results of an MDOF with real modal constants, close to the 1st resonance - $f_1 = 20Hz$ and $\eta_1 = 0.05$.
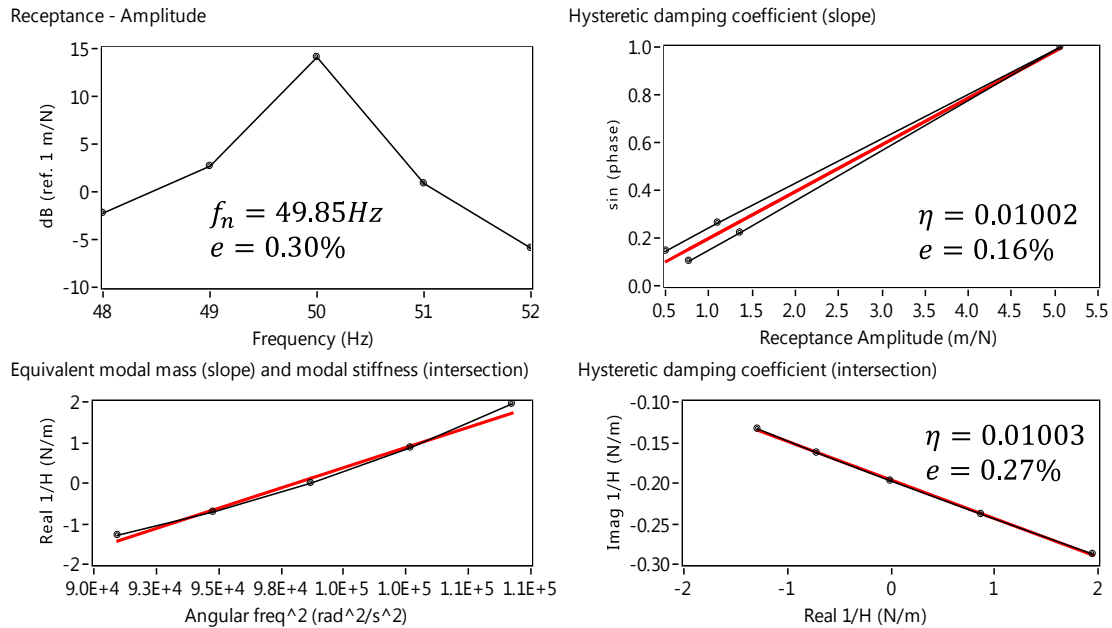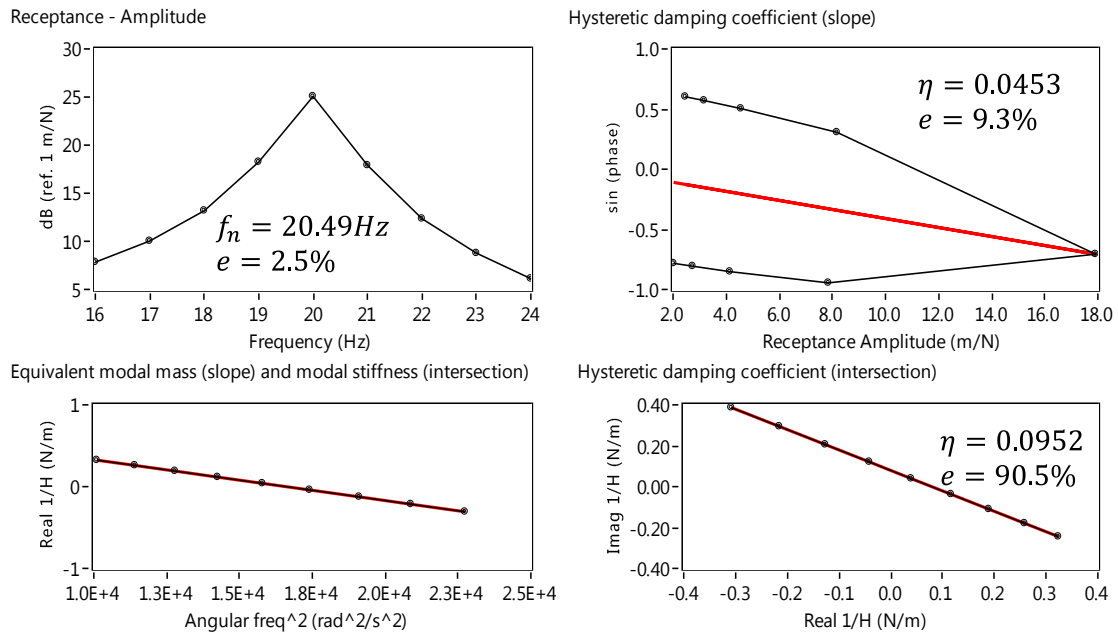

Fig. 4. Numerical results of an MDOF with real modal constants, close to the 2nd resonance - $f_2 = 50Hz$ and $\eta_2 = 0.01$.
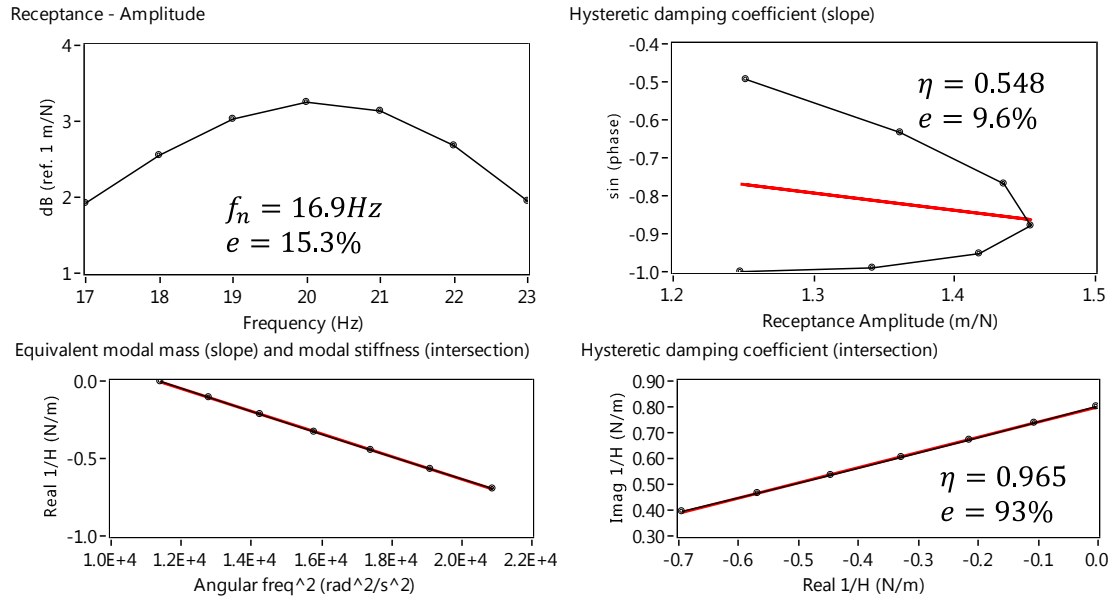
3.4. SDOF with a Complex Modal Constant

An imaginary part was added to the SDOF's modal constant of the system presented earlier in section 3.2, making it a complex quantity. The greatness of the imaginary part was deliberately chosen to be equal to the greatness of its real counterpart in order to amplify its effect. The results for the modal identification are shown in Fig. 5, in which it can be seen that the method of the "slope" produced a much more accurate result for the hysteretic damping factor (9% error) than the method of the "intersection" (91% error) - at least for the system values presented in table 1 - even if the data points on the right-bottom corner plot are displaced in a linear pattern. The estimate of the natural frequency is still quite accurate (2.5% error).
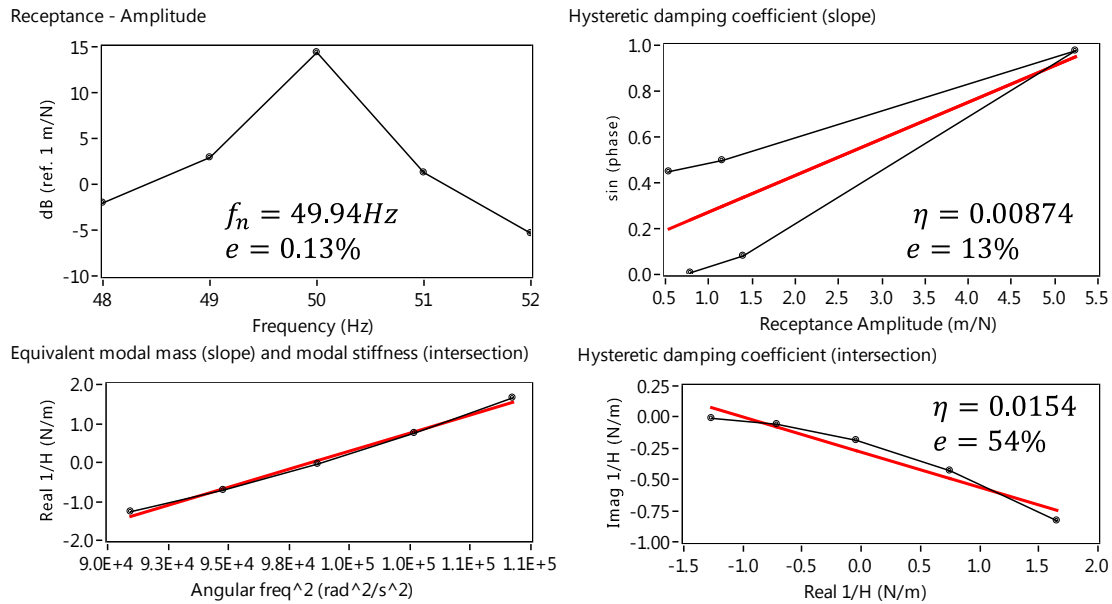

Fig. 5. Numerical results of an SDOF with a complex modal constant - $f = 20Hz$ and $\eta = 0.05$.

3.5. MDOF with Complex Modal Constants and a "Heavily" Damped Mode

One of the problems associated to many of the modal identification methods – and the one presented herein is not exempt from this – is that they are mostly effective for lightly damped systems. In this section, an MDOF with complex modal constants and a "heavily" damped mode (mode 1 at 20Hz with a hysteretic damping factor 10x greater than in the previous sections) is discussed. Figs. 6 and 7 are close-ups at the 20Hz and 50Hz resonances, respectively. Again, the method of the "slope" produced much better results (10% error) than the method of the "intersection" (93% error). This error was even smaller than the one obtained for the 1st mode's natural frequency (15% error), which typically is the most accurate quantity to determine.
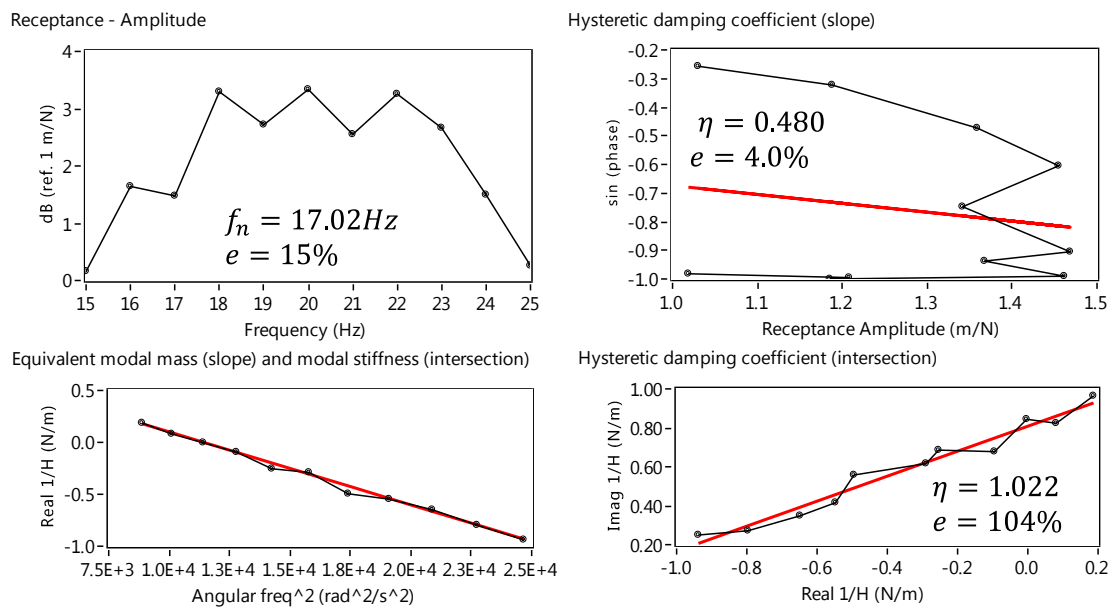
Fig. 6. Numerical results of an MDOF with complex modal constants, close to the 1st resonance (heavily damped) - $f_1 = 20Hz$ and $\eta_1 = 0.5$.
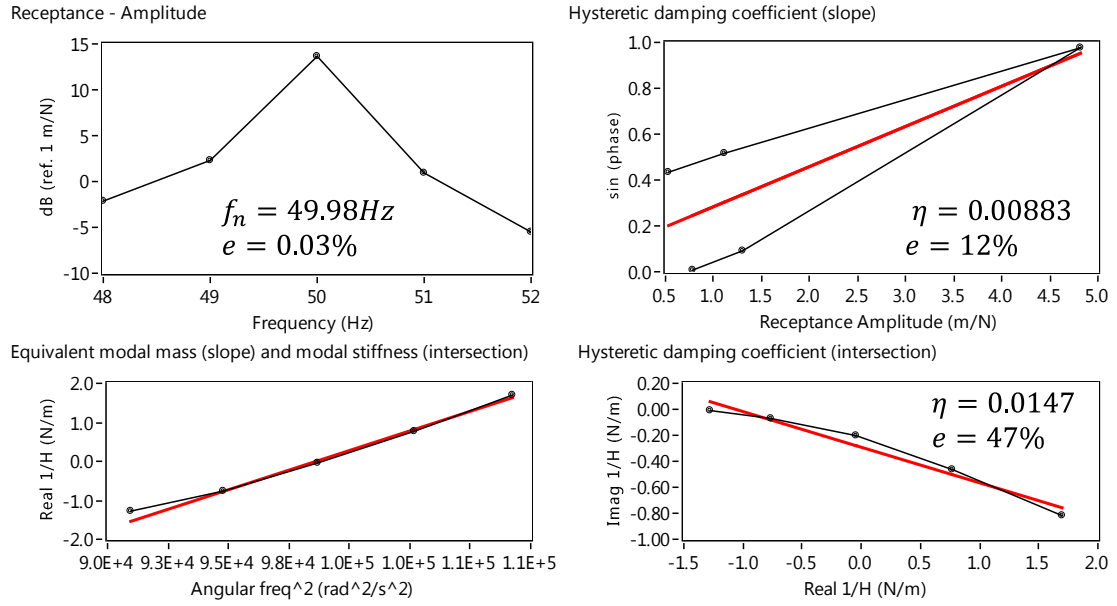

Fig. 7. Numerical results of an MDOF with complex modal constants, close to the 2nd resonance - $f_2 = 50Hz$ and $\eta_2 = 0.01$.

3.6. MDOF with Complex Modal Constants, a "Heavily" Damped Mode and Noise

The final numerical simulation adds ±10% random noise to the data points of the previous example (MDOF, complex modal constants and 1st mode at 20Hz "heavily" damped). Results are presented in Figs. 8 and 9. Again, the method of the "slope" produced much better results (4% error) than the method of the "intersection" (104% error). Nevertheless, it must be acknowledged that the selection of the data points to be included in the analysis is crucial for the method of the "slope" to work effectively. If the data points are not carefully chosen, erratic results may be obtained. This can be assessed by evaluating the quality of the linear fit, which can be done visually or, more rigorously, by means of the coefficient of determination.
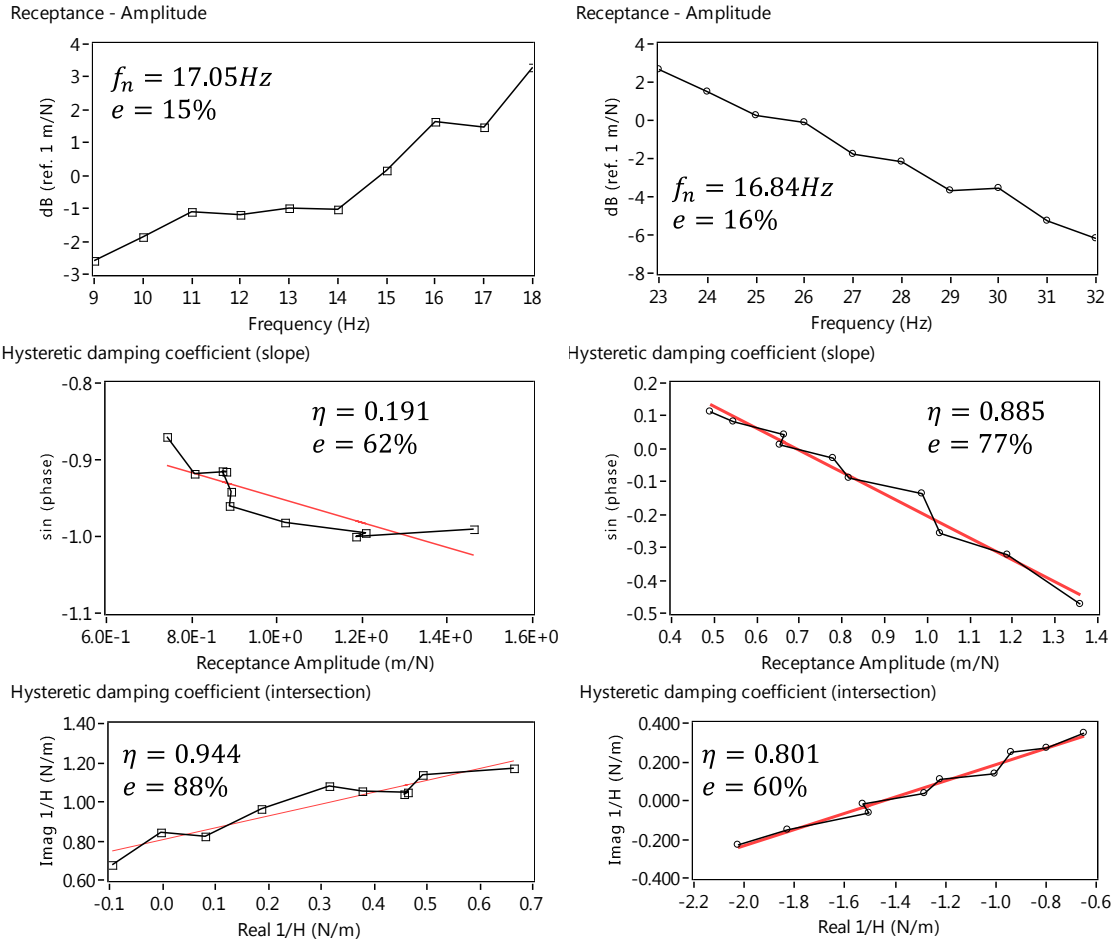

Fig. 8. Numerical results of an MDOF with complex modal constants and noise, close to the 1st resonance (heavily damped) - $f_1 = 20Hz$ and $\eta_1 = 0.5$.

Fig. 9. Numerical results of an MDOF with complex modal constants and noise, close to the 2nd resonance - $f_2 = 50Hz$ and $\eta_2 = 0.01$.

An alternative way for the identification of the modal damping in the method of the "slope" under the presence of noise, consists in making two independent identifications. The first identification is made made at the left side of the natural frequency and the second identification at the right side of the natural frequency. Next, the averaged value is determined. The results from this approach are presented in Fig. 10 and table 2. In this example, 10 data points were selected each time, for consistency purposes, neglecting the "zig-zag" points that appear on the method of the "slope" in Fig. 8 (between 18 and 23 Hz).

It can be observed that, by executing these two independent identifications, it was possible to obtain a fairly good estimate of the hysteretic damping factor with the method of the "slope" (from the average, see results in bold in table 2). Furthermore, because only data points on the same side of the natural frequency were used at each time, this approach seems to be less prone to the experience of the user when choosing the data points.

Fig. 10. Numerical results of an MDOF with complex modal constants and noise, close to the 1st resonance - $f_1 = 20Hz$ and $\eta_1 = 0.5$. Plots on the left correspond to identifications made using data points on the left of the natural frequency; plots on the right correspond to identifications made using data points on the right of the natural frequency.

Table 2 Numerical results of an MDOF with complex modal constants and noise, close to the 1st resonance - $f_1 = 20Hz$ and $\eta_1 = 0.5$.

Case	This paper's method (slope)				Im(1/H) vs Re(1/H) (Intersection)	
	f_n (Hz)	e (%)	$\boldsymbol{\eta}$	$\boldsymbol{e}$ (%)	η	e (%)
Left	17.05	15	0.191	62	0.944	88
Right	16.84	16	0.885	77	0.801	60
Average	16.95	15	**0.538**	**8**	0.873	75

4. Experimental Examples

4.1. Experimental Setup and Data Acquisition

Assessment of the method of the "slope" (Eq. (14)) was made using experimental results from a carbon fibre rectangular plate in a free-free suspended configuration. Again, results were compared to those obtained from the method of the "intersection" (Eq. (17)). In both cases, the modal hysteretic damping factors were determined using Eq. (8). The modal stiffness and modal mass were estimated from a least-squares best fit from Eq. (24), in which the stiffness parameter is estimated from the interception of the line with the imaginary axis and the modal parameter is estimated from the slope of the line. The natural frequency was finally determined from (25).

The composite plate used in this study is formed by 8 unidirectional plies with $[0/90]_{2S}$ layup. Each layer is made of an epoxy resin impregnated with carbon fibre satin weave Cytec Cycom 934-373KT300. The dimensions of the test plate are, approximately, 360x262x3mm.

Free-free boundary conditions were simulated in the lab, suspending the specimen plate vertically by 2 nylon strings attached to two 1mm diameter holes at a distance of 50mm from the corners and 5mm from the top edge. Frequency response functions (FRFs) were measured using a National Instruments DAQ-9234 analogue input data acquisition module on a National Instruments cDAQ-9174 USB chassis. The first channel was allocated to the excitation force (measured with a PCB 208C01 force transducer) and the other three were used to measure the acceleration responses at three different locations (measured with PCB 352C22 lightweight teardrop accelerometers).

An electromagnetic shaker LDS V201 was used to produce the excitation signal, at a single coordinate, with a copper pushrod 60mm long attached to the force transducer at the other end. A white noise excitation signal ranging from 0 to 800Hz was generated and amplified using a NI 9263 analogue output module and an LDS PA25E power amplifier.

Signal Express 2012 from National Instruments was used to process and record the results. The FRFs were recorded under the form of Receptance and a Hanning window was used during the signal acquisition.

In the following sections, 4.2 and 4.3, the results for the identification of three natural frequencies and hysteretic damping factors are discussed. The same four types of pictures as those discussed in chapter 3 are analysed, as well as the same parameters: the hysteretic damping factors and the natural frequencies. The main difference now is that there are three

receptance curves available for the modal identification, since three accelerometers at three different locations were used.

4.2. Single-curve Identification

Figs. 11, 12 and 13 present the results for the experimental example described in section 4.1, in which the modal identification is performed on each receptance curve individually. The averaged results from the three curves have been summarized in table 3 and compared to the values obtained with the modal identification software BETAlab [13]. The results from BETAlab were taken as reference values in the comparison.
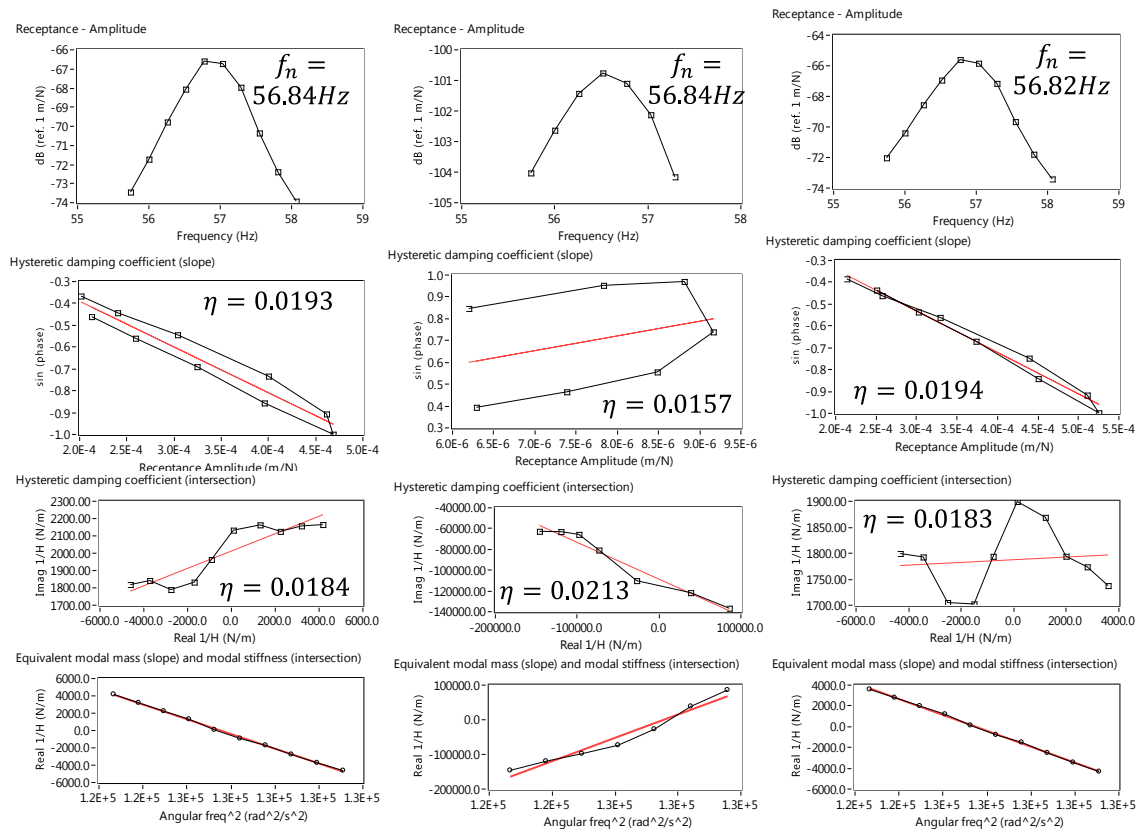
Fig. 11. Single-curve experimental results close to the 1st resonance - $f_1 \cong 57 Hz$.
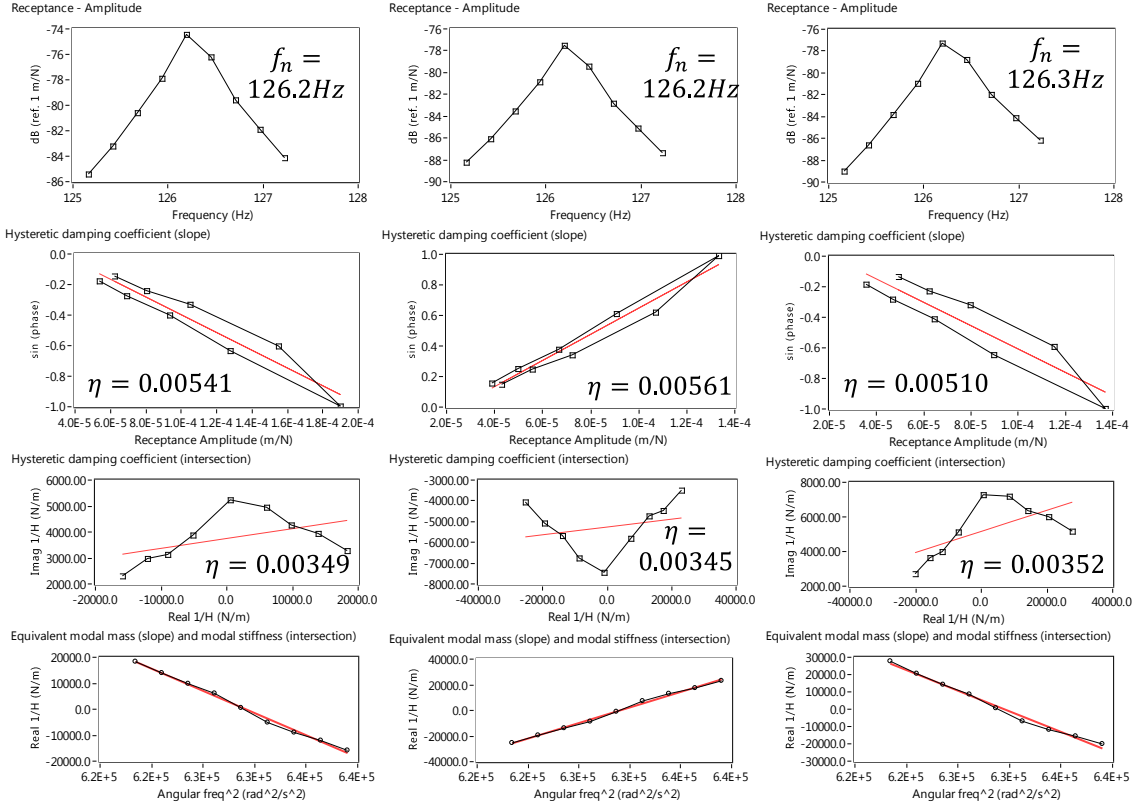
Fig. 12. Single-curve experimental results close to the 2nd resonance - $f_2 \cong 126 Hz$.
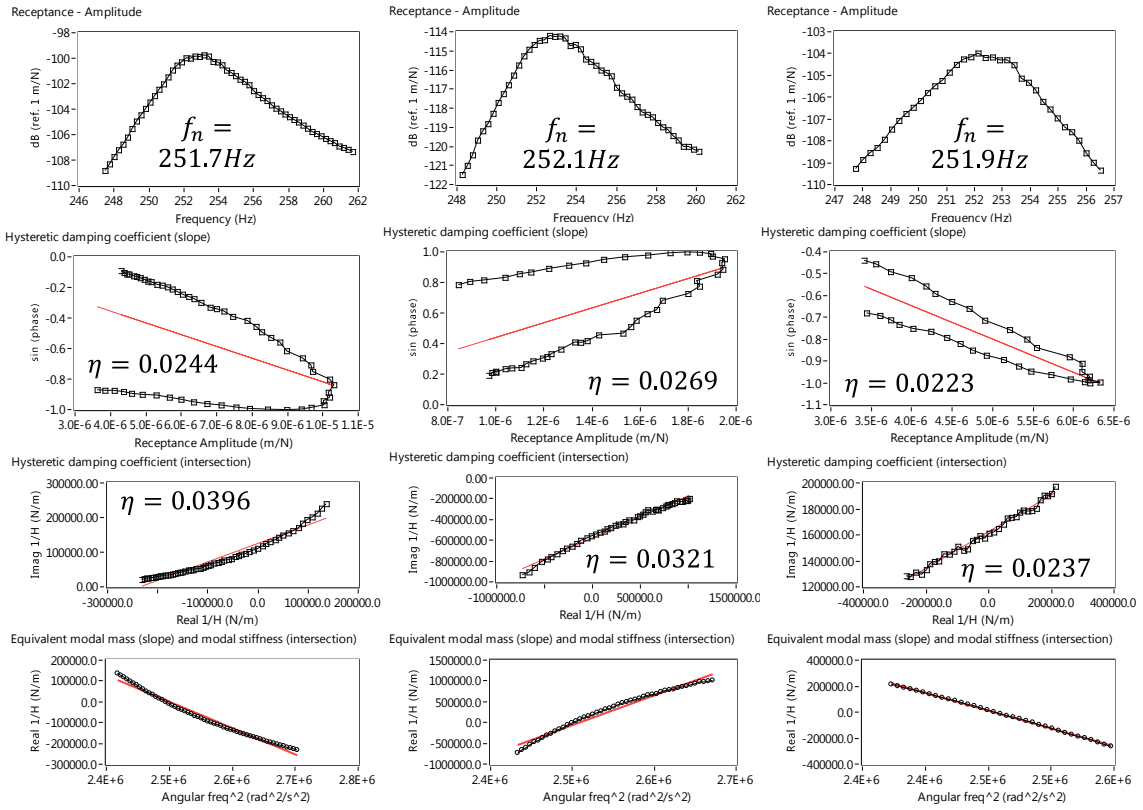
Fig. 13. Single-curve experimental results close to the 3rd resonance - $f_3 \cong 252 Hz$.

Table 3 Summary of the experimental results shown in Figs. 11, 12 and 13.

Mode	BETAlab	This paper's method (slope)		Im(1/H) vs Re(1/H) (Intersection)	
	η	η	e (%)	η	e (%)
1st, ~57Hz	0.0184	0.0181	1.63%	0.0193	4.9%
2nd, ~126Hz	0.00410	0.00537	31%	0.00349	15%
3rd, ~252Hz	0.0226	0.0245	8.4%	0.0318	41%

All the three methods produced consistent results in terms of the hysteretic damping factor for the 1st mode shape.

Concerning the 2nd mode shape, the discrepancies were quite larger between the three methods, but it must be observed that the damping factor itself is quite smaller, which means that its estimate is also more sensitive to experimental uncertainty.

Regarding the 3rd mode, it is suggested- again - that the method of the "slope" is less sensitive to more heavily damped systems than the method of the "intersection", either because the error is smaller (in comparison to the BETAlab results) or because the hysteretic damping estimate from one curve to the other has less variations (the sample standard deviation was determined at 0.00230 for the method of the "slope" and 0.00795 for the method of the "intersection").

4.3. Multiple-curve Identification

A first attempt to perform the modal identification with all the curves at the same time was made. These results are presented in Fig. 14 and table 4. First of all, it must be noted that the modal identification was made having the method of the "slope" as reference. A few problems occurred, reason why not all the results have been presented:

- When performing the modal identification, it was noted that some slopes were positive whereas others were negative. This is due to the different signals (positive or negative) of the modal constants, as observed earlier in section 3.3. This effect had to be corrected so that all the slopes presented the same signal while measuring the hysteretic damping factors;

- One of the signals on the 1st mode was polluting the data too much and preventing the results to be accurate. This was noted because the curves on the method of the "slope" were not superimposing each other. This happened in a more pronounced way

for the 3rd mode, preventing the hysteretic damping from being determined with any 2 curves at the same time;
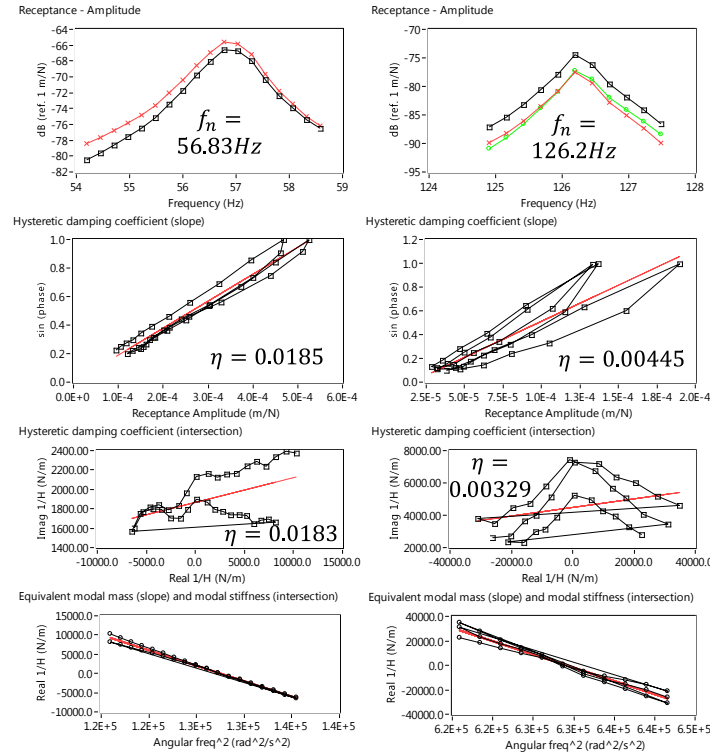
Fig. 14. Multiple-curve experimental results – 1st and 2nd modes.

Table 4 Summary of the experimental results shown in Figs. 11, 12 and 13.

Mode	BETAlab	This paper's method (slope)		Im(1/H) vs Re(1/H) (Intersection)	
	η	η	e (%)	η	e (%)
1st, ~57Hz	0.0184	0.0185	0.54%	0.0183	0.54%
2nd, ~126Hz	0.00410	0.00445	8.5%	0.00329	20%
3rd, ~252Hz	0.0226	n.a.	n.a.	0.0249	10%

5. Conclusions

A novel method for the identification of the modal damping factor from FRFs was presented. It is based on the dissipated energy per vibration cycle and on the well-known method of the inverse. For lightly damped systems with conveniently spaced modes, it allows determining the modal damping factors in a simple way from the receptance FRFs and with a reasonable degree of accuracy. Due to lack of a better term, it was called method of the "slope" within the context of this paper.

In comparison to the traditional method of the inverse, in which the damping coefficient is determined from the imaginary part of the dynamic stiffness (herein called method of the "intersection"), the method of the "slope" seemed to be slightly more robust to numerical instability. Also, this method seemed to be much less sensitive to the modal constants, especially when these are complex quantities with large imaginary parts. Both methods work better for lightly damped systems, although the method of the "slope", again, seemed to perform better with more heavily damped systems. However, in terms of limitations, the method of the "slope" is more sensitive to the experience of the user than the method of the "intersection", because the number of points chosen to the right or to the left may have a strong influence on the quality of the identification, whereas for the method of the "intersection" this is not an issue.

When using multiple curves at the same time, the method of the "slope" failed to produce satisfactory results. However, the combination of this technique with others like the Characteristic Response Function [14] that act as a way of "normalising" the FRF, might be a feature to explore in the future.

Finally, although it was not the objective of this paper, one important observation was that the signal of the slope in the method of the "slope" is dependent on the signal of the modal constant. It's "sharpness" also depends on the imaginary part of the modal constant (the smaller the imaginary part, the "sharper" the visual aspect of the plot). These observations indicate that representation of $\sin(\theta)$ vs the amplitude of the receptance can be correlated with the modal constants as well, although further developments are still required.

Acknowledgements

References

[1]   N.M.M. Maia, J.M.M. Silva, Theoretical and Experimental Modal Analysis, Research Studies Press and John Wiley and Sons, Somerset, 1997.

[2]   A. Sadhua, B. Hazraa, S. Narasimhana. Decentralized modal identification of structures using parallel factor decomposition and sparse blind source separation, Mech. Syst. Signal Process., 41 (2006) 396-419.

[3]   A. Siu-Kui, Uncertainty law in ambient modal identification—Part I: Theory, Mech. Syst. Signal Process., In Press, Corrected Proof, Available online 31 October 2013

[4]   L. Thien-Phu, P. Paultre, Modal identification based on the time–frequency domain decomposition of unknown-input dynamic tests, Int. J. Mech. Sci, 71 (2013) 41-50.

[5]   L. Cheng, D. Zheng, The identification of a dam's modal parameters under random support excitation based on the Hankel matrix joint approximate diagonalization technique, Mech. Syst. Signal Process. 42 (2014) 42-57.

[6]   J.L. Zapico-Valle, M. García-Diéguez, R. Alonso-Camblor, Nonlinear modal identification of a steel frame, Eng Struct, 56 (2013) 246-259.

[7]   J.A. Gonilha, J.R. Correia, F.A. Branco, E. Caetano, A. Cunha, Modal identification of a GFRP-concrete hybrid footbridge prototype: Experimental tests and analytical and numerical simulations, Compos. Struct., 106 (2013) 724-733.

[8]   L. Zhang, R. Brincker, P. Andersen, An Overview of Operational Modal Analysis: Major Development and Issues, Proceedings of the 1st International Operational Modal Analysis Conference (IOMAC), April 26-27, Copenhagen, Denmark, 2005.

[9]   D.J. Ewins, Modal Testing: Theory and Practice, Research Studies Press And John Wiley and Sons, Letchworth, 1984.

[10]   B.J. Lazan, Damping of materials and members in structural mechanics. Pergamon Press, Oxford, 1968.

[11]   D. Montalvão, A.M.R. Ribeiro, J.D. Silva, R.A. Cláudio, Experimental Measurement of the complex Young's modulus on a CFRP laminate considering the constant hysteretic damping model, Compos. Struct., 97 (2013) 91-98.

[12]   L. Meirovitch, Elements of Vibration Analysis, McGraw-Hill, International Edition, 1986.

[13]   D. Montalvão, A Modal-based Contribution to Damage Location in Laminated Composite Plates, PhD thesis, Instituto Superior Técnico, Technical University of Lisbon, Portugal, 2010.

[14]   J.M.M. Silva, N.M.M. Maia, A.M.R. Ribeiro, Structural Dynamic Identification with Modal Constant Consistency using the Characteristic Response Function (CRF), Machine Vibration, 5 (1996) 83-88.